COHESIVE ZONE MODEL FOR DUCTILE FRACTURE - COMPARISON OF PREDICTION WITH EXPERIMENT

Guoyu Lin*, Alfred Cornec* and Karl-Heinz Schwalbe*

Simulation of 3D crack growth using a cohesive zone model (CZM) was carried out for a side-grooved compact tension and a surface crack tension specimen of Aluminium 2024FC. Detailed finite element calculations were conducted by assuming crack growth only along the crack plane (mode I). For comparison, 2D plane strain simulation is also presented. Load, displacement and crack growth histories are predicted and compared with experiment. It will be shown that the 2D approximation appears to agree reasonably with experimental results and the 3D calculation gives very good agreement with test data. Numerical results show that the CZM is a workable computational model which involves only a few microstructurally motivated phenomenological parameters for crack growth simulation.

INTRODUCTION

It is well known that crack tip constraint strongly affects the crack growth resistance. Numerical study by Brocks et al. (1) has shown that a strong interaction between in-plane and out-of-plane constraint effects on crack-front fields in a 3D configuration cannot be captured in the plane strain analyses. Several proposals (references 2-4) have been suggested to quantify the crack tip constraint. However, they are still not suitable to quantify the constraint influence on crack resistance. Therefore, a full 3D crack growth simulation is desired to study the constraint effect on fracture behavior. Recently, a CZM has been described and applied to simulate ductile fracture process (references 5-9). In this paper, detailed finite element calculations based on the CZM are carried out for simulating 3D crack growth in a side-grooved compact tension (CTsg) specimen and a semi-elliptical surface crack panel (SCT) under tension made from Aluminium 2024FC. The numerical analysis was conducted under mode I condition and it was assumed that crack grows in the crack plane only. The phenomenon of the canoe-effect in the surface crack tension panel observed in the experiment is well reproduced by the simulation.

* GKSS-Forschungszentrum Geesthacht GmbH, Max-Planck-Str., D-21502 Geesthacht, Germany

PROBLEM FORMULATIONS

The Cohesive Zone Model

Figure 1a defines the general mechanics problem: a band of inelastic deformation emanates from a crack/notch in a component. The band is localized in that its thickness is much smaller than any other lengths characterizing the component. The inelasticity in the band is modeled as an array of springs (cohesive zone) with a nonlinear traction-separation law of

$$T=T(\delta). \tag{1}$$

The cohesive energy is then given by

$$\Gamma = \int_0^{\delta_f} T(\delta)d\delta, \tag{2}$$

where δ_f is the maximum separation. In the present study, a constant traction-separation law is used, i.e.

$$T(\delta)= T_o\,, \tag{3}$$

where T_o is the cohesive stress. It may be interpreted as the "micro" material strength. The fracture mechanism is represented by a local critical fracture energy, Γ_o,

$$\Gamma= \Gamma_o. \tag{4}$$

It is noted that Eq. (4) is assumed for the given fracture mechanism. Γ_o represents the "micro" material toughness. Both Γ_o and T_o are thought to be *material dependent* only. Fig. 1b graphically interprets the effect of constraint on the fracture resistance based on the CZM. Instead of being viewed as a singularity, fracture, or any localized damage band, is now a gradual stretching under the constant cohesive stresses.

Geometries and Finite Element Models

The dimensions of the side-grooved CT specimen used in the analysis were W=50mm, a_o/W=0.5, B=5mm and B_{net}=3mm (40% side grooved). Because of symmetry only one-half of the geometry needs to be analyzed. Figure 2a displays the finite element mesh for the half geometry of CTsg specimen. The element arrangement in the vicinity of the crack front is shown in Fig. 2b. The regular small element size is 0.167mm. The dimensions of a SCT specimen were 2W=100mm, t=10mm, a_o/c_o=0.868 and a_o/t=0.466. Figure 3a displays the finite element mesh for the one-quarter geometry of the SCT specimen. The element arrangement in the vicinity of the crack tip is shown in Fig. 3b. The smallest element size is about 0.25mm. Eight-node brick elements with 2x2x2 selectively reduced integration

scheme was used in the calculations. The FE mesh for the specimens under study consisted of about 7000 elements and 7000 nodes. The specimens were made from Aluminium 2024FC. The material constants employed in the calculations were $E=72000N/mm^2$, $\nu=0.3$ and $\sigma_{0.2}=80.7N/mm^2$, and the true stress-strain curve was used. The two cohesive zone parameters Γ_0 and T_0 were chosen to be 10N/mm and $420N/mm^2$ according to Cornec et al. (5). Note that the element sizes in the two meshes are not the same. However, it has been demonstrated in the previous studies (6, 8) that the CZM has the advantage of mesh size independence.

RESULTS

Figure 4 displays load-CMOD curves for the CT specimen. The thick solid line indicates the experimental test curve. For the 3D case, CMOD is measured at the center plane of the specimen. However, no difference is observed between the center and surface planes. Fig. 4 shows that the 3D prediction by the CZM agrees well with the experimental records. The 2D simulation underestimates the experimental curve. Note that the load in 2D plane strain case was calculated using net thickness B_{net}. Fig. 5 plots the CMOD as a function of crack extension Δa. Again, the values of CMOD were measured at the center plane. Solid line indicates CMOD versus Δa at the center plane. The dashed line is for Δa near the free surface. Crack initiation is found at the free surface. Also, it is seen that CMOD at crack initiation agrees well with the experiment. Moreover, it is observed that the crack extension near the free surface is much faster than that of the specimen center, due to the side-groove raising the crack tip constraint at the free surface.

Figure 6 compares predicted and experimental load-CMOD curves for the SCT specimen. The solid circles and open circles indicate the experimental test points of two specimens. The 3D prediction by the CZM agrees well with the experimental records. Fig. 7 displays the CTOD δ_5 versus CMOD for $\vartheta=0°$, 30° and 90°. Note that δ_5 measures the displacement at the crack tip over a gage length of 5mm. $\vartheta=0°$ corresponds to the free surface. The maximum δ_5 is obtained at the free surface. δ_5 decreases from $\vartheta=0°$ to 90°, which is much different from the through crack specimen. This also implies that the constraint along the crack front changes significantly for the surface crack. Fig. 8 shows the numerically predicted crack surface at two load levels of CMOD=0.766 and 0.909mm. The thick solid line indicates the initial crack front. Crack initiation is found at $\vartheta=90°$. With increasing the load, the canoe-shaped crack surface is formed. The crack propagates largely along the crack front from $\vartheta=25°$ to 90°. The maximum crack growth is found at

ϑ=25° to 40°. Up to highest applied load, no crack growth at ϑ=0° was observed. Unfortunately, there is no experimental record at this load level for comparison.

CONCLUDING REMARKS

Ductile crack growth for a CTsg and a SCT specimen was simulated by using an elastic-plastic continuum model with a cohesive zone model. The fracture process, which may be due to void nucleation, growth and coalescence, is confined to a narrow material strip (a cohesive material) and characterized by a traction-separation law. The crack tip constraint is captured by the model in a natural way. Numerical results show that the CZM is a workable computational model which involves only two microstructurally motivated phenomenological parameters (Γ_o and T_o) for crack growth simulation. Moreover, the proposed model has the advantage of mesh independence and is easy to implement into a finite element code and finite element calculation is very stable. Approaches which build in the fracture process hold promise for predictions of crack growth behavior from small scale yielding to large scale yielding.

REFERENCES

(1) W. Brocks and J. Olschewski, *International Journal of Solids and Structures*, Vol.22, 693-708, 1986.
(2) W. Brocks *et al.*, *Nuclear Engineering Design*, Vol.112, 1-14, 1989.
(3) Z.-Z. Du and J.W. Hancock, *Journal of the Mechanics and Physics of Solids*, Vol.39, 555-567, 1991.
(4) N.P. O'Dowd and C.F. Shih, *Journal of the Mechanics and Physics of Solids*, Vol.39, 989-1015, 1991.
(5) A. Cornec, H. Yuan and Guoyu Lin, in *Numerical predictions of deformation processes and the behavior of real materials*, Proceedings of the 15th RISO International symposium on material science, 269-275(1994).
(6) Guoyu Lin and A. Cornec, 27. Vortragsveranstaltung des DVM-Arbeitskreises Bruchvorgänge, Köln, 1995.
(7) H. Yuan, Guoyu Lin and A. Cornec, *Journal of Engineering Materials and Technology*, ASME Transactions, Vol. 116, 1-9, 1996.
(8) Guoyu Lin and A. Cornec, *28. Vortragsveranstaltung des DVM Arbeitskreises Bruchvorgänge*, Bremen, Feb., 1996.
(9) Guoyu Lin, Yun-Jae Kim, A. Cornec and K.-H. Schwalbe, *Performance of Strength Mis-Matched Welded or Bonded Joints*, 2nd International Symposium on Mis-Matching of Welds, Lüneburg, Germany, 1996.

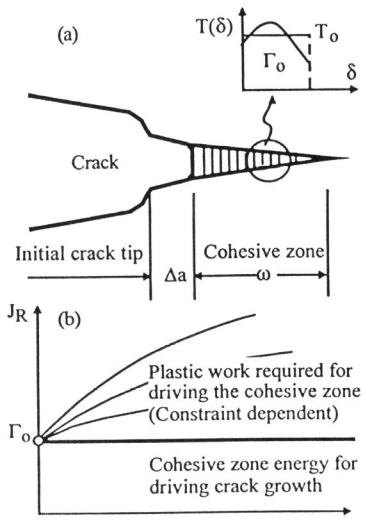

Fig. 1 Schmatic of the CZM for fracture.

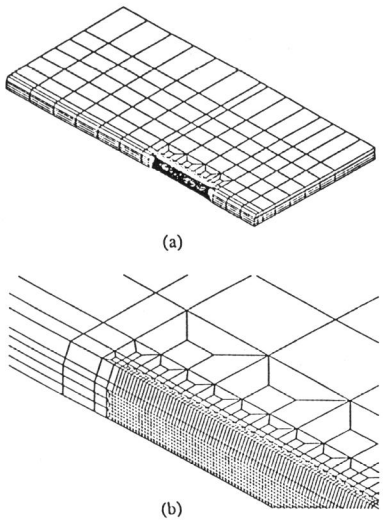

Fig. 2 FE mesh for CTsg.

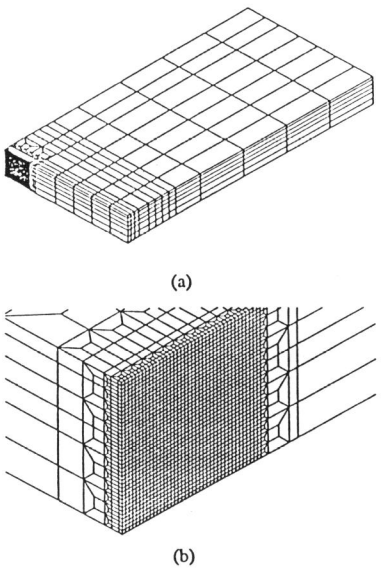

Fig. 3 FE mesh for SCT.

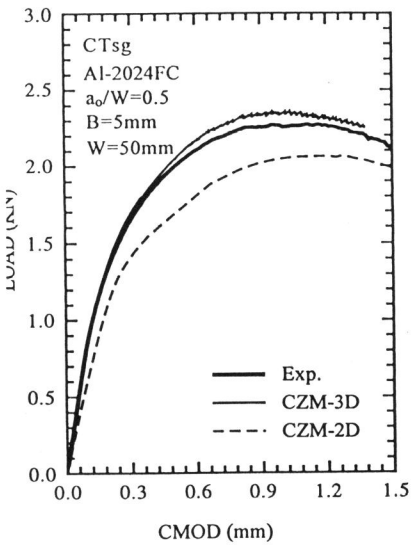

Fig. 4 δ_5-CMOD curves for CTsg.

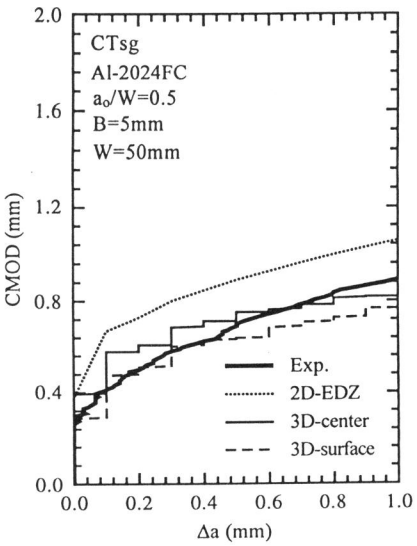

Fig. 5 Load-CMOD curves for CTsg.

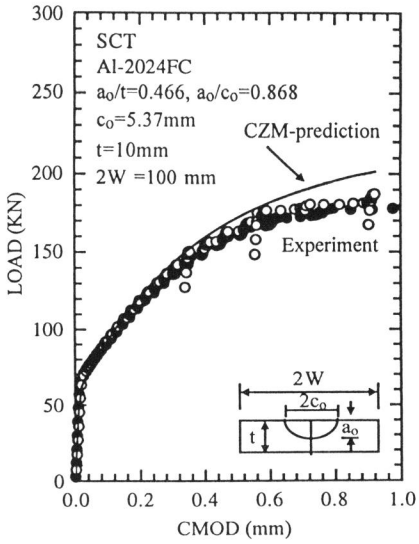

Fig. 6 Load-CMOD curves for SCT.

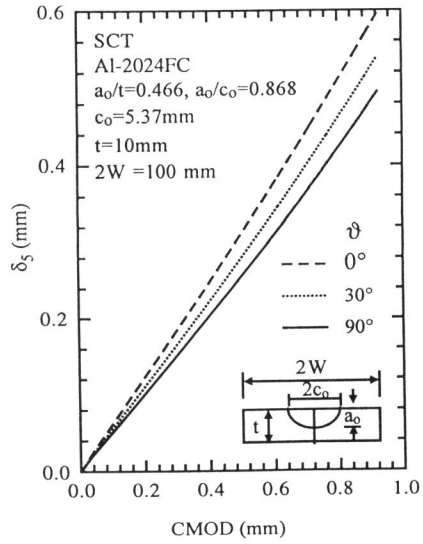

Fig. 7 δ_5-CMOD curves for SCT.

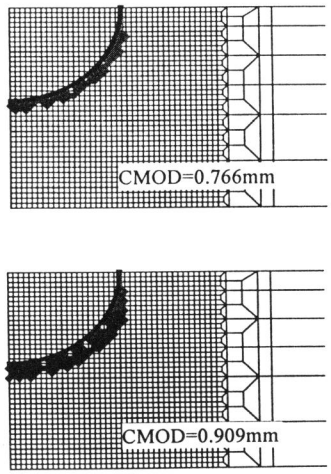

Fig. 8 Predicted crack surface.